EPFL

Bachelor project

Project Report

Flow simulation in ophtalmic arteries for intra-arterial chemotherapy against Retinoblastoma

---

Lily Gilibert 345357

Spring Semester 2024

Contents

Background and Objective

This project falls within the improvement of the treatement for retinoblastoma, a form of eye cancer. Currently, the most effectve treatment involves intra-arterial chemotherapy injection with a catheter. However, the currently used catheters are too large to avoid complications while going into the ophthalmic artery. Therefore it is the current clinical practice to stop the catheter at the entrance to the ophthalmic artery and perform injection there, supposedly being less efficient.
The objective of this project is to simulate and compare the flow distribution for a conventional and novel magnetically controlled catheter when insterted into the ophthalmic artery.

1 Preprocessing of the model

1.1 Simulation Preparation and Initial Challenges

The 3d model of the geometry of the carotid and ophthalmic artery was obtained by manually segmenting a patient CT scan.
The initial stage of the project involved preparing the geometry for simulation, which presented significant challenges:

- Phantom Usability: The provided phantom represented only the outer shell of the vessel, which is unsuitable for fluid dynamics simulation in COMSOL. Successful simulation requires the full vessel geometry to appropriately apply blood properties and conduct the analysis.
- File Compatibility: The geometry files were in .stl format and other types that are unsuitable with COMSOL. This necessitated conversion to a more suitable format such as .step.

To address the first issue, two approaches can be employed :

- CAD Modification: It was attempted to reconstruct the vessel from the phantom using Fusion 360's "fill hole" function.
- COMSOL Cap Faces: A more effective method involved using COMSOL's "cap faces" function, as detailed in a tutorial, to encapsulate the vessel geometry and discard the phantom. This technique proved to be more efficient.

For the second issue, initial challenges were encountered with the file formats. COMSOL prefers .step files, but the phantom's CAD file could not be exported in this format for unknown reasons, necessitating the continued use of .stl files. The vessel's original file was in .obj format, which is also not optimal for COMSOL. These files were repaired and converted in Fusion 360, following a tutorial, and then reimported into COMSOL as .step files. However, quality issues persisted during import and meshing, particularly with the vessel model, which showed numerous errors due to the .step export. Some of these issues were irreparable without a better model.

Ultimately, the phantom model was successfully repaired in Fusion 360, exported to COMSOL, and the vessel was extracted using the "Cap Faces" function. After this extensive troubleshooting, a test simulation was conducted using water as a proxy material to approximate blood dynamics and simplify the model.

Simulation Parameters :
Based on [3], the average volume flow rate of blood in the carotid artery is approximately 267.77 ml/min. This value is the average value obtained by color duplex sonography on 13 healthy adults subjects. According to [1], the average volume flow rate in the ophthalmic artery is 10.37 ml/min. This value is the average value obtained by phase contrast MRI on 28 healthy adults and 23 elderly subjects. This preparatory work laid the foundation of the rest of the project.

- 3D Laminar flow module with stationary study
- Material : water
- Fine meshing

- Inlet with flow rate boundary conditions : $\dot{Q} = 4.463 \cdot 10^{-6}$ m^3/s
- First outlet (carotid) with a pressure BC : $p = 0$ (reference pressure is $P_{ref} = 0$)
- Second outlet (ophtalmic) with a flow rate BC : $\dot{Q} = 1.728 \cdot 10^{-7}$ m^3/s

The parameters used are those of a simple flow simulation in a tube.

Challenges in implementing test simulation
The initial approach to simulating flow involved setting a boundary condition (BC) on the first outlet (carotid artery), intended to represent the difference between the flow rates at the inlet and the outlet in the ophthalmic artery. However, this model setup consistently failed to converge, accompanied by a specific error: "There is no feature constraining the pressure. A pressure constraint is required to specify the pressure level." To address this issue, it was assumed that the pressure difference between the inlet and outlet of the carotid artery was negligible. Consequently, a zero pressure BC was applied at the first outlet.
Although this assumption made the simulation work, it introduced potential inaccuracies in the model's results.

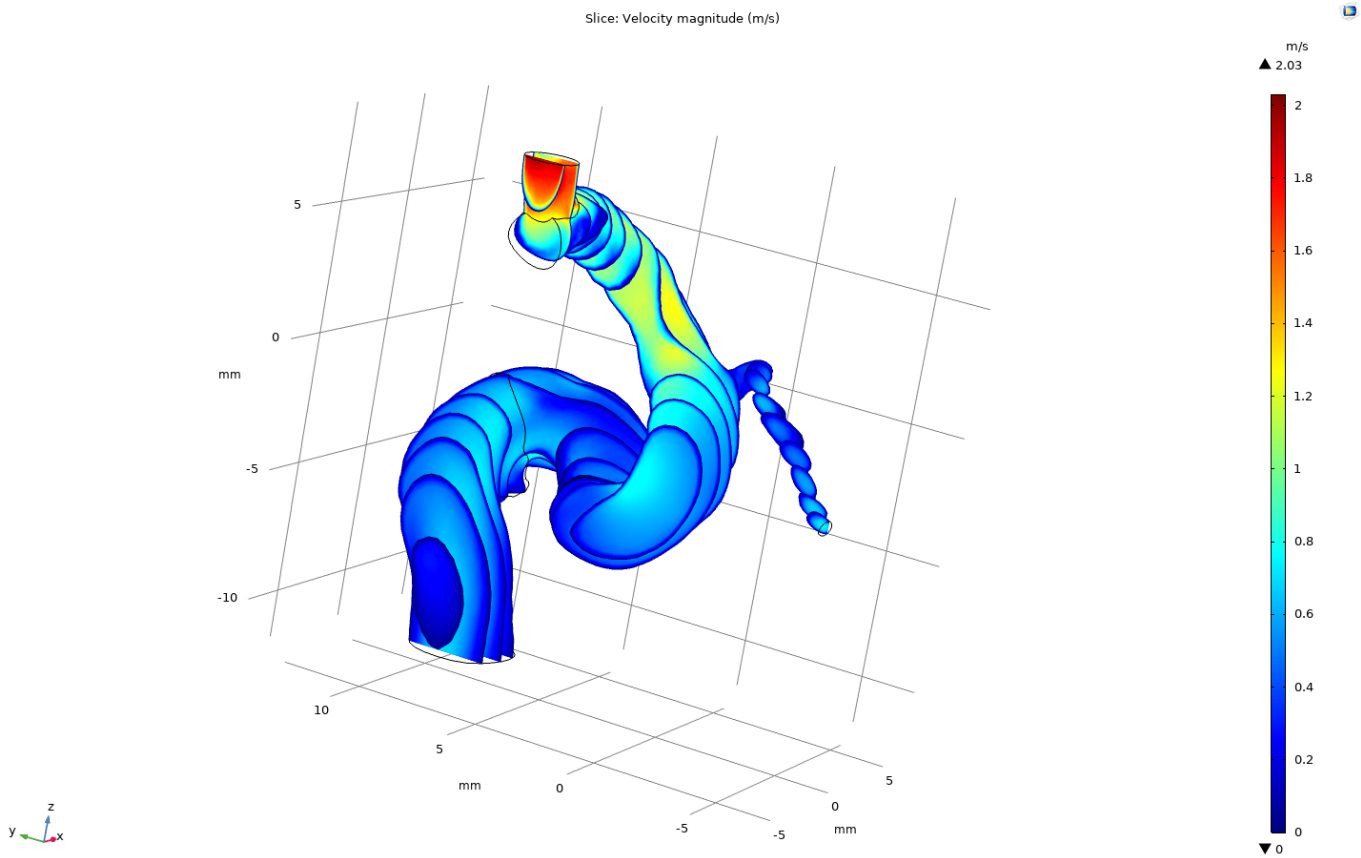

Figure 1: Flow simulation of water in the vessel

1.2 Initial Results

The model shows a peak flow velocity reaching approximately 65 cm/sec. These values are compared against documented values by [8], where the peak systolic flow velocity was reported as 45.1 ± 7.8 cm/sec.
The simulation suggests that blood flow velocities in the model are higher than those observed in empirical studies. This discrepancy could be attributed to several factors:

- Model Simplifications : The simulation might incorporate assumptions and simplifications that affect fluid dynamics, leading to variations in flow velocity.

- Boundary Conditions : The boundary conditions set for the simulation, particularly the zero pressure BC at the first outlet, may influence the velocity outcomes, potentially accounting for the elevated flow rates observed.
- Geometric Accuracy : The fidelity of the vessel geometry used in the simulation relative to actual human anatomy could also impact the flow dynamics. The difference could also be due to the anatomy of a patient being an outlier.

Fine-tuning the model or adjusting the boundary conditions could provide better simulation results. Consulting with domain experts or exploring more detailed studies might also enhance our model's accuracy in replicating real-life physiological conditions.

2 Simulation Parameters

The values for the parameters used in this report were chosen based on a combination of scientific literature and empirical data. These parameters are listed below, along with their significance, to maintain consistency across the different sections throughout the report. Specific references for each parameter are provided in the relevant sections of the report.

Name	Expression	Value	Description
P_{in}	-	$100[mmHg]$	Average pressure in carotid artery
$\dot{Q}_{in}$	-	$4.463e-6[m^3/s]$	Average flow rate in the carotid before the opthalmic artery
$\dot{Q}_{opt}$	-	$1.728e-7[m^3/s]$	Average flow rate in the opthalmic artery [1]
$\dot{Q}_{car}$	$\dot{Q}_{in}-\dot{Q}_{opt}$	$4.2802e-6[m^3/s]$	Average flow rate in the carotid artery after the ophtalmic artery
T_{ref}	-	310 [K]	Average blood temperature
R_{car}	-	$22[mmHg\cdot s/ml]$	Carotid arterial resistance
R_{opt}	-	$200.8[mmHg\cdot s/ml]$	Opthalmic arterial resistance
C_{car}	-	$25.6e-5[ml/mmHg]$	Carotid arterial capacity
C_{opt}	-	$0.4e-5[ml/mmHg]$	Opthalmic arterial capacity
Z_{car}	-	$7.3327e8[kg/(m^4\cdot s)]$	Carotid arterial compliance
Z_{car}	-	$1.0708E11[kg/(m^4\cdot s)]$	Opthalmic arterial compliance
R_1	$R_{car}/(R_{car}+Z_{car})$	0.2	Ratio carotid
R_2	$R_{opt}/(R_{opt}+Z_{opt})$	0.8	Ratio opthalmic
τ_{car}	$R_{car}\cdot C_{car}$	$0.005632[s]$	Time constant of the carotid
τ_{opt}	$R_{opt}\cdot C_{opt}$	$8.032e-4[s]$	Time constant of the opthalmic
f	-	$1[Hz]$	Heart frequency
$Z_{eq,car}$	-	$3.6642e9[kg/(m^4\cdot s)]$	Equivalent impdedance in the carotid artery
$Z_{eq,opt}$	-	$1.3385e11[kg/(m^4\cdot s)]$	Equivalent impdedance in the opthalmic artery

3 Test simulation with water

3.1 Simple model - 1^{st} version

Due to the complex geometry of the original vessel model, which required considerable time and computational resources during meshing and flow simulation, a simplified model was developed using Fusion 360. This model consists of a truncated cone that mimics the average diameter of the carotid artery, connected to a smaller cylinder representing the average diameter of the ophthalmic artery (refer to Figure 2).
Initially, a test flow simulation was conducted on this model. Subsequently, modifications were made to incorporate a hole in the ophthalmic artery segment, which simulates the magnetic tip of the catheter.

3.1.1 Model parameters

3.1.1.1 CAD dimentions

As said in the introduction of the section, the dimensions of the truncated cone are based on the vessel. The bifurcation of the ophtalmic artery is situated at about two third of the lenght (see Figure 2 for visualisation).

- Base diameter : $D_b = 4$ mm
- Top diamater : $D_t = 3$ mm
- Lenght : $L = 20$ mm
- Smaller tube diameter : $d = 0.8$ mm

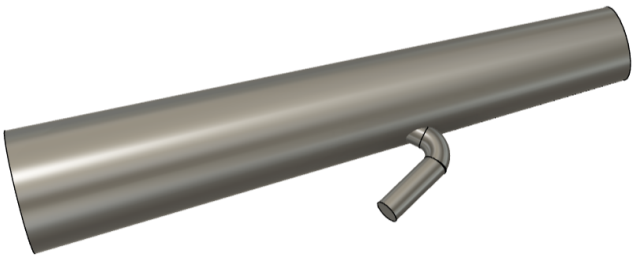

Figure 2: Simple model CAD

3.1.1.2 Magnetic tip

The magnetic tip was modeled as a cylinder with a diameter of $D_{mt} = 200\mu$m and a length of $L_{mt} = 500\mu$m (refer to Figure 3 for visualization).
The magnetic tip is located in the opthalmic artery at the exit of the first turn, as shown in Figure 4.
The location of the magnetic tip was chosen to be in the middle of the vein in the curve, where it would logically block the most flow.

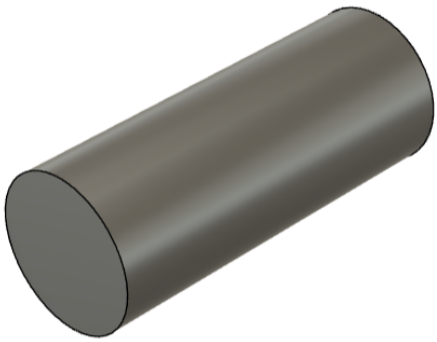

Figure 3: Magnetic tip CAD model

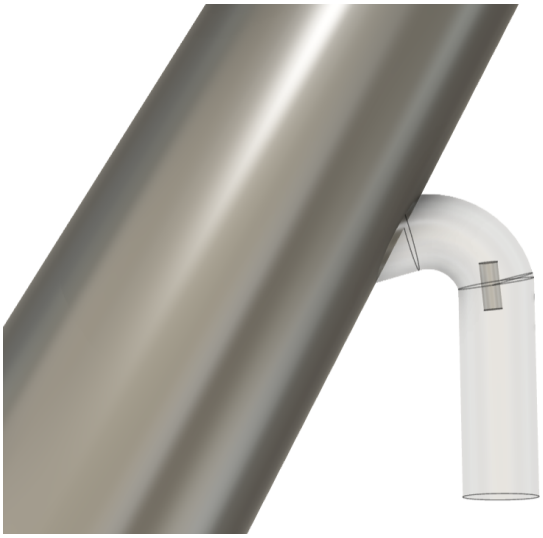

Figure 4: Magnetic tip location in the ophtalmic artery

3.1.1.3 Comsol parameters

The same Comsol parameters are applied for the next simulations :

- 3D Laminar flow module with stationary study
- Material : water
- Fine meshing
- Inlet is the base diameter with a flow rate boundary conditions : $\dot{Q}_{in} = 4.463 \cdot 10^{-6}$ m^3/s
- First outlet is the top diameter and the smaller tube with a pressure BC : $p = 0$ (reference pressure is $P_{ref} = 0$)
- Second outlet is the smaller tube with a flow rate BC : $\dot{Q}_{opt} = 1.728 \cdot 10^{-7}$ m^3/s

3.1.2 Flow simulation without magnetic tip

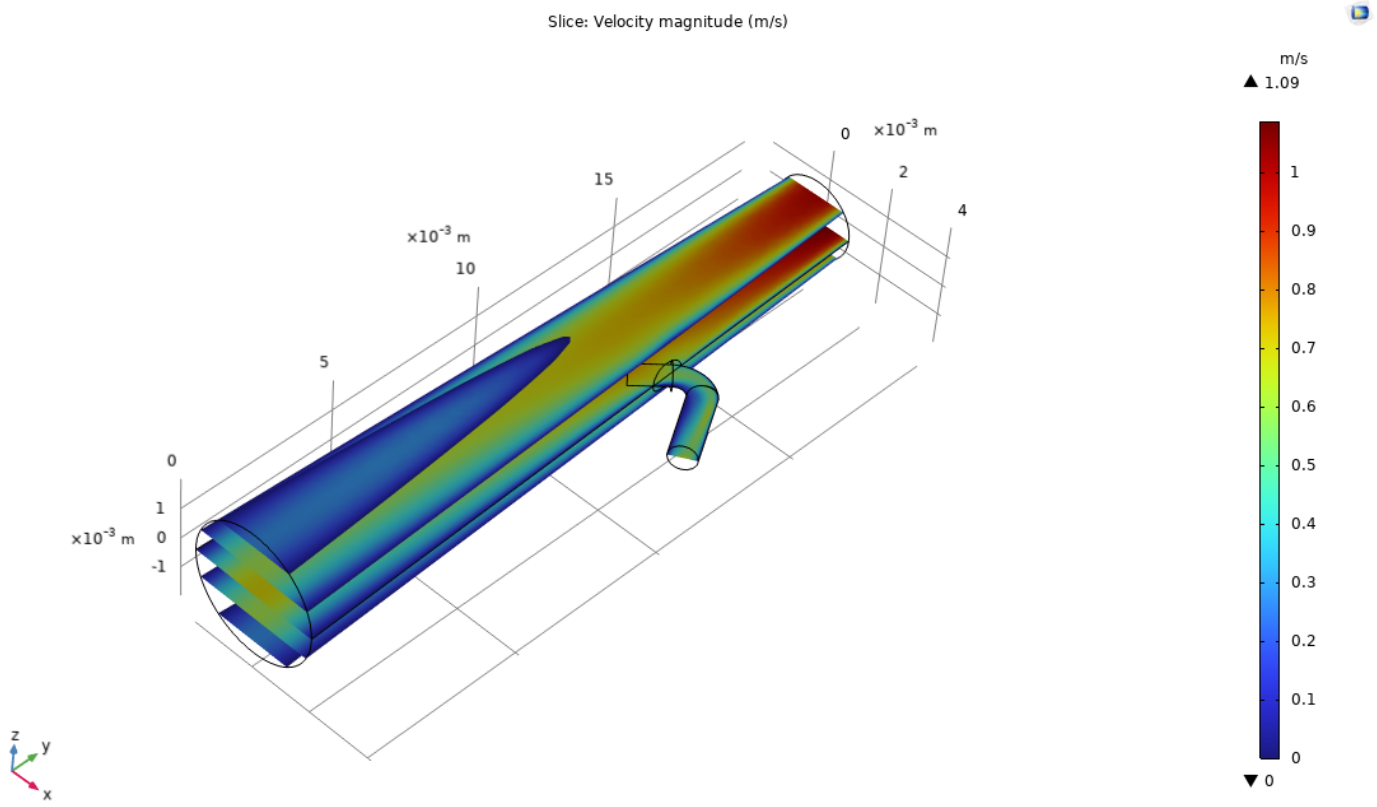

Figure 5: Flow simulation of water in the simple model

Analysis
In Figure 5, the simulation results show a maximum flow velocity of approximately 62 cm/sec in the ophthalmic artery. These values are consistent with those observed in the more complex vessel model shown in Figure 1, suggesting that the simplified model provides a reasonable approximation of the original.

3.1.3 Flow simulation with magnetic tip

Analysis
As presented in Fig. 6, the presence of the magnetic head within the ophthalmic artery does not significantly disrupt the flow. Although there is a brief obstruction when the flow interacts with the magnetic head, the flow velocities swiftly return to their typical levels shortly thereafter.
This outcome suggests that the magnetic head's impact on flow dynamics might be less significant than predicted. Several factors could contribute to this observation:

- Material properties : Using water as a proxy might enhance false results as blood does not act like water in very small vessels.
- Boundary conditions : The boundary condtions are overly simplified and might not fit the fluid dynamics at play.
- Geometry : The simple model can be revised to better represent the complex geometry of the vessel

3.1.4 Improvements

Upon reflection, the initial simplified model used for the simulation has been identified as needing improvements to better reflect real-world conditions. The following changes are proposed to enhance its accuracy:

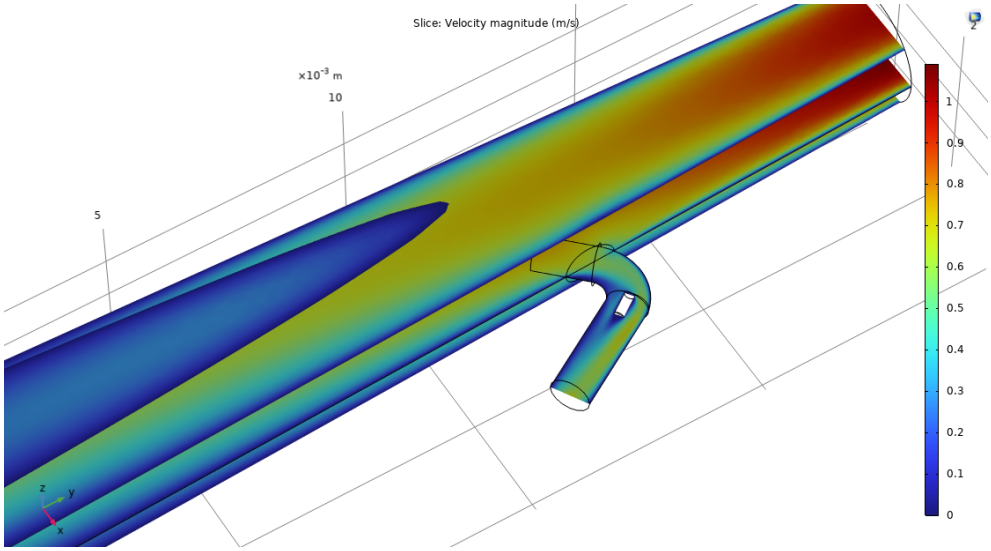

Figure 6: Simulation of the simple model with the magnetic tip

1. Adjustments to Dimensions:

   The diameter of the ophthalmic artery in the model will be adjusted to match the minimum diameter observed in the actual vessel.

2. Modification of Boundary Conditions:

   - The inlet will have an average flow rate boundary condition (BC) to better simulate the average physiological flow entering the artery.
   - The outlets will utilize a pressure BC, specifically employing a three-element Windkessel model. This model helps mimic the downstream vascular resistance and compliance, providing a more physiologically accurate depiction of pressure dynamics at the exits.

These updates to the boundary conditions are designed to enhance the simulation's fidelity to actual physiological behaviors, thereby improving the overall accuracy and relevance of the model's predictions.

3.2 Three-element Windkessel model

The three-element Windkessel (3WK) model is widely utilized in cardiovascular biomechanics. The 3WK model effectively calculates the pressure in vessels, allowing for an accurate measurement of the pressure drop across the model.

Using [5], the 3WK modelise the flow in the vessel as an electrical circuit consisting of a resistance R, a capacitor C and an impedance Z_c :
Therefore the equation of the model linking the pressure drop to flow rate is :

$$\frac{\partial p}{\partial t} + \frac{p}{RC} = \frac{Q}{C}(1 + Z_c/R) + Z_c\frac{\partial Q}{\partial t} \tag{1}$$

and knowing that we are in steady-state flow, we have $\frac{\partial Q}{\partial t} = 0$, which yields :

$$\frac{\partial p}{\partial t} + \frac{p}{RC} = \frac{Q}{C}(1 + Z_c/R) \tag{2}$$

We also know the equivalent impedance of the circuit Z_{eq} is :

$$Z_{eq} = \frac{R + Z_c + j\omega R Z_c C}{1 + j\omega RC} \tag{3}$$

$$|Z_{eq}| = \sqrt{\frac{(R + Z_c)^2 + (\omega R Z_c C)^2}{1 + (\omega RC)^2}} \tag{4}$$

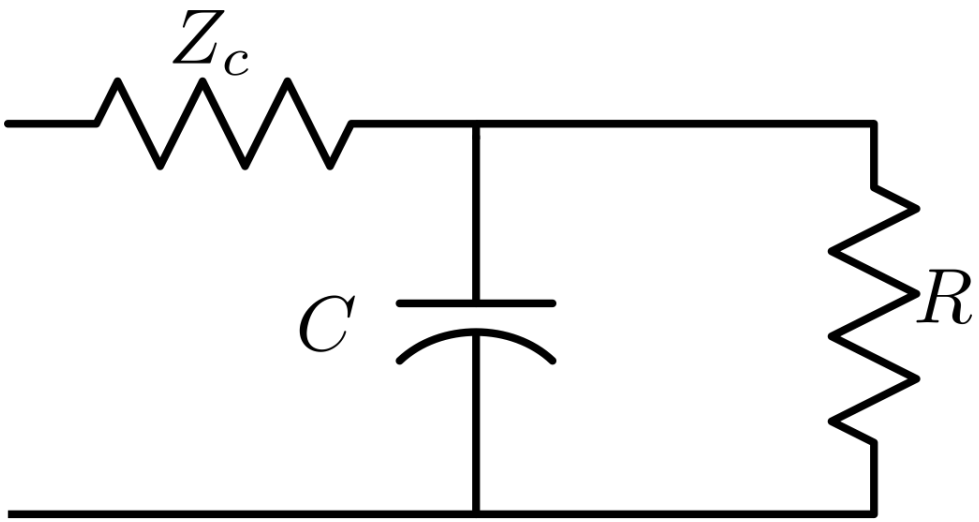

Figure 7: Three-element Windkessel model

There is two possibilities to implement this differential equation in COMSOL :

1. Implement the whole differential equation with the global equation module
2. Discretize the function and implement the discretization using the **timestep** function

3.2.1 Global equation module

The Windkessel model was incorporated into the simulation through COMSOL's global equation module. The equations implemented are as follows :

$$\dot{p}_{car} + \frac{p_{car}}{R_{car}C_{car}} - \frac{Q_{car}}{C_{car}}(1 + Z_{car}/R_{car}) = 0 \qquad \dot{p}_{opt} + \frac{p_{opt}}{R_{opt}C_{opt}} - \frac{Q_{opt}}{C_{opt}}(1 + Z_{opt}/R_{opt}) = 0 \tag{5}$$

These equations aim to dynamically update the pressure and flow rate at each iteration. A probe was used to measure the flow rate value at each iteration, with subsequent updates to the pressure values via the differential equations.
We visualise the simulation in Figure 8.

Analysis :
The execution of this simulation is computationally intensive, taking approximately 5 to 6 hours to complete. This extensive computation time is due to the complexity involved in continuously updating the pressure and flow rates throughout the simulation iterations.
According to Figure 9, the average flow rate at the carotid outlet (Boundary probe 1) is around $4.3 \cdot 10^{-6}$ $[m^3/s]$ and the average flow rate at the opthalmic outlet (Boundary probe 2) is around $0.2 \cdot 10^{-6}$ $[m^3/s]$.

3.2.2 Discretization

The second technique involves discretizing the differential equation. Similar to the first approach, it utilizes the global equation module to update the pressure. However, rather than using probes to measure and update the flow rate at each iteration, this method defines the flow rate through an equation based on the pressure.
The discretization in the time model is :

$$\frac{p^{n+1} - p^n}{\Delta t} + \frac{p^{n+1}}{RC} = \frac{Q(1 + Z_c/R)}{C} \tag{6}$$

which leads to :

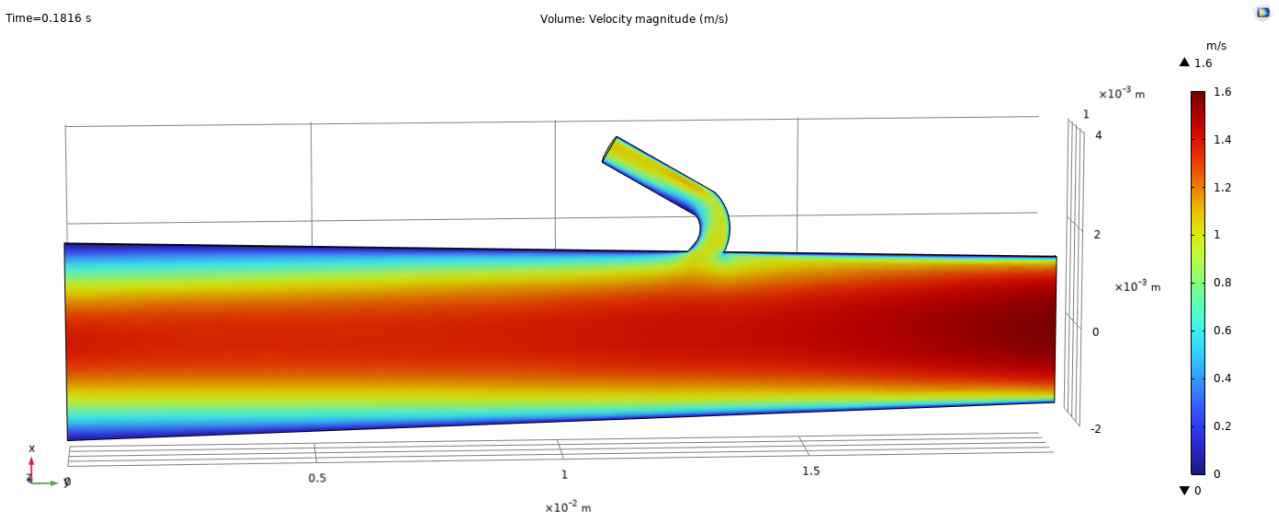

Figure 8: Flow simulation tip using the global equation module

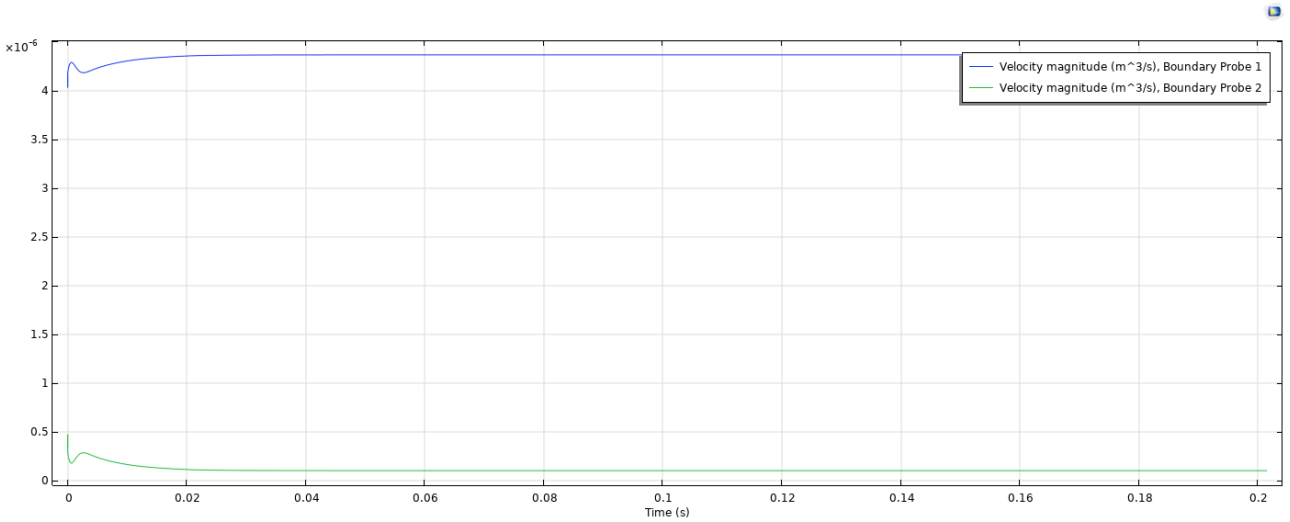

Figure 9: **Flow rate at the outlets**

$$p^{n+1} = \frac{p^n + \frac{q^n \Delta t}{C} \frac{R+Z_c}{R}}{1 + \Delta t/\tau} \qquad \tau = RC \tag{7}$$

We also have a relationship to link p^n to q^n at an instant t. Given Figure 7, we know that $\Delta q = \Delta p / Z_{eq}$. Thanks to that we can deduct initial values to solve our equations using the average flow rate of the carotid and opthalmic artery.

Knowing that the heart rate is around 60 bpm, we have that the frequency of the heart is about $f_{heart} = 1$ [Hz], which gives $\omega = 2\pi f_{heart} = 2\pi$ which we can use in (4).

To resume, we can modelise the blood flow with the sequences $p^{n+1}(p^n, q^n)$ and $p^n(q^n)$, with the intial conditons being the average flow in the vessels without the magnetic tip inside :

$$p_{car}^{n+1} = \frac{p_{car}^n + \frac{q_{car}^n \Delta t}{C_{car}} \frac{R_{car}+Z_{car}}{R_{car}}}{1 + \Delta t/\tau_{car}} \qquad q_{car}^n = \frac{p_{car}^n}{|Z_{eq,car}|} \tag{8}$$

$$p_{opt}^{n+1} = \frac{p_{opt}^n + \frac{q_{opt}^n \Delta t}{C_{opt}} \frac{R_{opt}+Z_{opt}}{R_{opt}}}{1 + \Delta t/\tau_{opt}} \qquad q_{opt}^n = \frac{p_{opt}^n}{|Z_{eq,opt}|} \tag{9}$$

Initial conditions for carotid and opthalmic:

$$p_{car}^0 = Q_{car} * |Z_{car}^{eq}| \qquad p_{opt}^0 = Q_{opt} * |Z_{opt}^{eq}| \tag{10}$$

The parameters $R_{car}, R_{opt}, C_{car}, C_{opt}$ are obtained from litterature ([7]).

Computing the model in COMSOL gives us the results shown in Figure 10.

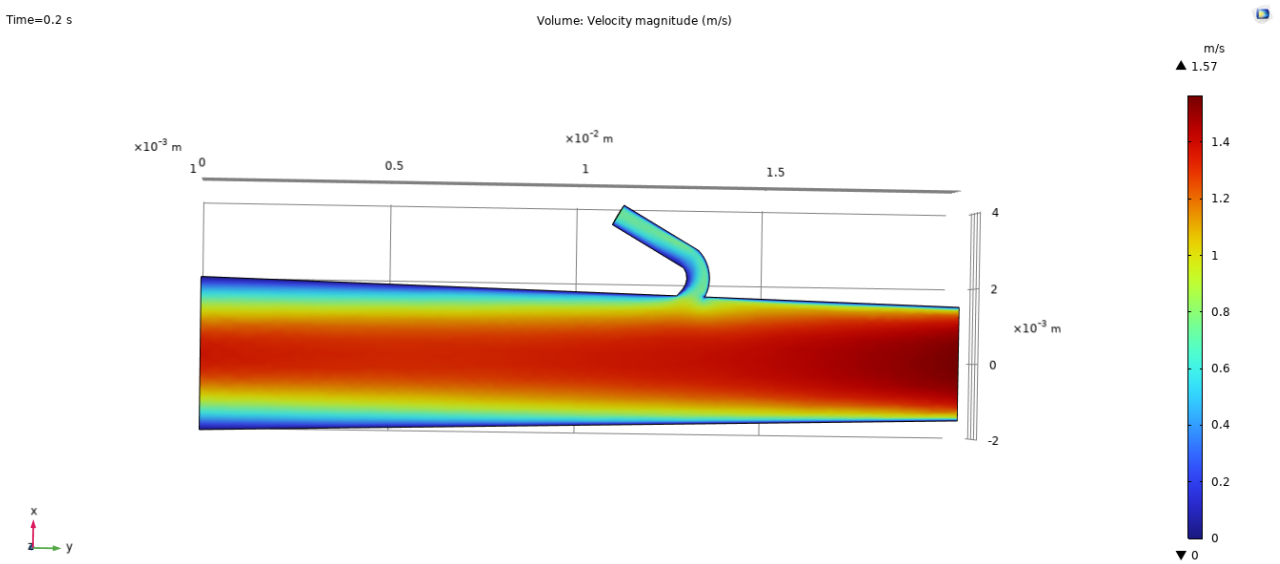

Figure 10: Flow simulation with discretized Windkessel model

Analysis :
As shown on Figure 11, the average flow rate for the carotid artery outlet of $4.40 \cdot 10^{-6}$ $[m^3/s]$ and the average flow rate at the ophtalmic outlet is $0.0616 \cdot 10^{-6}$ $[m^3/s]$

3.2.3 Comparaison of the two models

Outlet flow rate	Carotid $\dot{Q}_{car}$ $[m^3/s]$	Ophtalmic $\dot{Q}_{opt}$ $[m^3/s]$
ODE	$4.3 \cdot 10^{-6}$	$0.2 \cdot 10^{-6}$
Discretisation	$4.40 \cdot 10^{-6}$	$0.0616 \cdot 10^{-6}$
Literature	$4,45 \cdot 10^{-6}$ [3]	$0.114 \cdot 10^{-6}$ [8]

Comparison of Simulation Results:
When comparing the two simulation models, the values for the carotid artery closely match those reported in the literature for both models. This consistency suggests that both models are reliable for simulating flow in the carotid artery.
However, there are discrepancies in the values for the ophthalmic artery. In the first model, the flow values are approximately twice those found in the literature, indicating an overestimation. Conversely, the second model

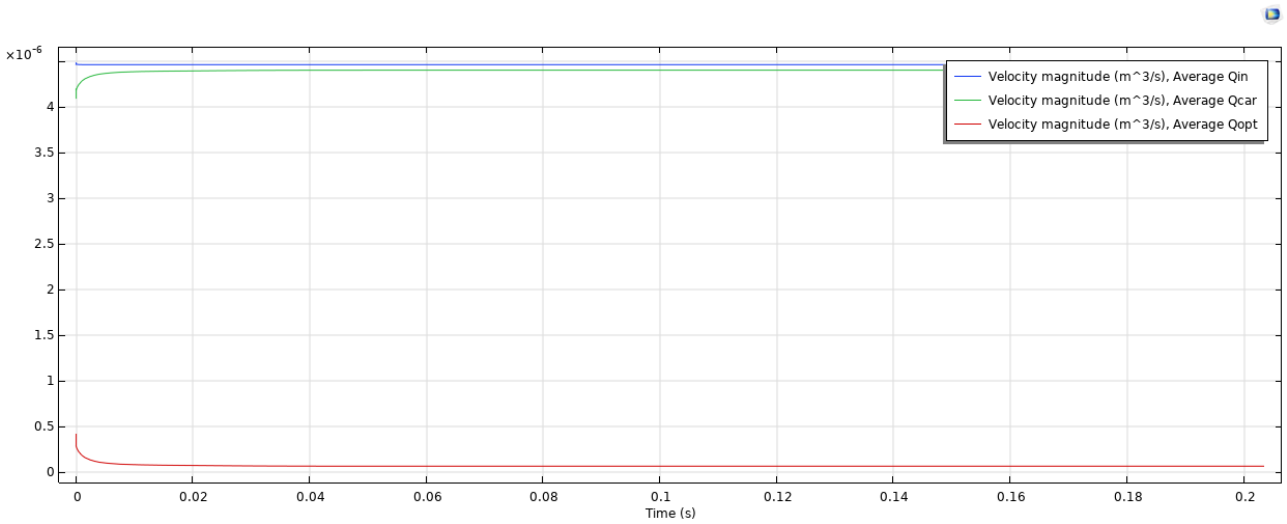

Figure 11: Flow simulation with discretized Windkessel model

has flow values that are about half of those reported in the literature, suggesting an underestimation. It is important to note that the order of magnitude are the same as in litterature.

Analysis:
These discrepancies highlight potential issues with each model's assumptions or parameter settings when applied to the ophthalmic artery. However, the computational time for the discretized model is significantly shorter than that of the continuous model. Thus, the project will proceed using the discretized model to decrease computational time and cost. Further simulations could,however ,be made with the continuous model and compared.

3.3 Flow simulation comparison

In this section, we will analyze how the flow in the ophthalmic artery is affected by different configurations of medical instruments. Specifically, we will compare the behavior of the flow under three conditions:

1. A control simulation with no obstacles to the flow. (Figure 12)
2. A simulation using a magnetic tip with a radius of 0.2 μm and a length of 0.5 μm. (Figure 13)
3. A simulation using a catheter with a radius of 0.4 μm.(Figure 16)

This comparison will help us understand the impact of each instrument on the flow dynamics within the ophthalmic artery.

3.3.1 Control simulation

This simulation is used to compare the values of the average flow rate at each inlet and outlets to litterature and to have a base simulation to comnpare the simulations with magnetic tips.
The results of this simulaton can be found in **3.2.2**.

3.3.2 Simulation with magnetic tip of 0.2 μm radius and 500 μm length

The results from this simulation (Figure 14) are much more aligned with what one would expect. In previous simulations, the flow in the ophthalmic artery increased and was barely impacted by the magnetic tip, indicating that the simulation parameters were likely incorrect.
Now, we observe that the velocity in the ophthalmic vessel is much slower and does not accelerate towards the end of the vessel.

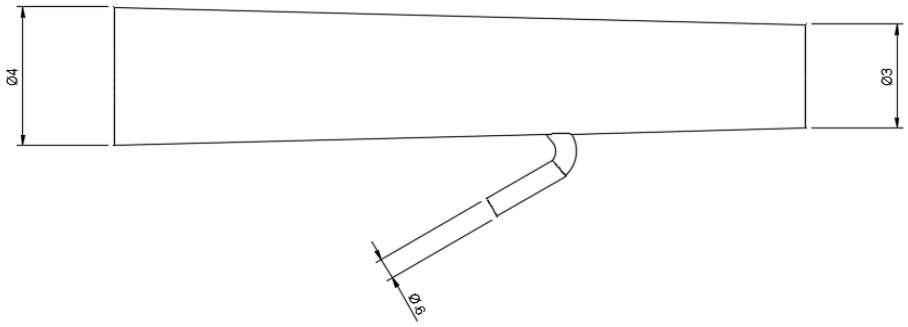

Figure 12: Control model CAD

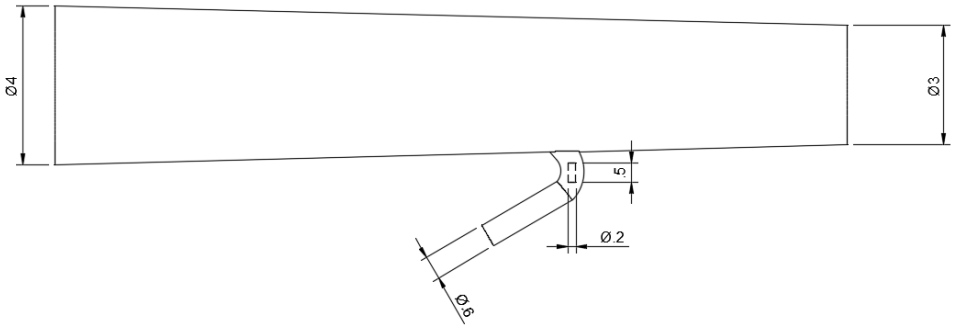

Figure 13: Model with magnetic tip CAD

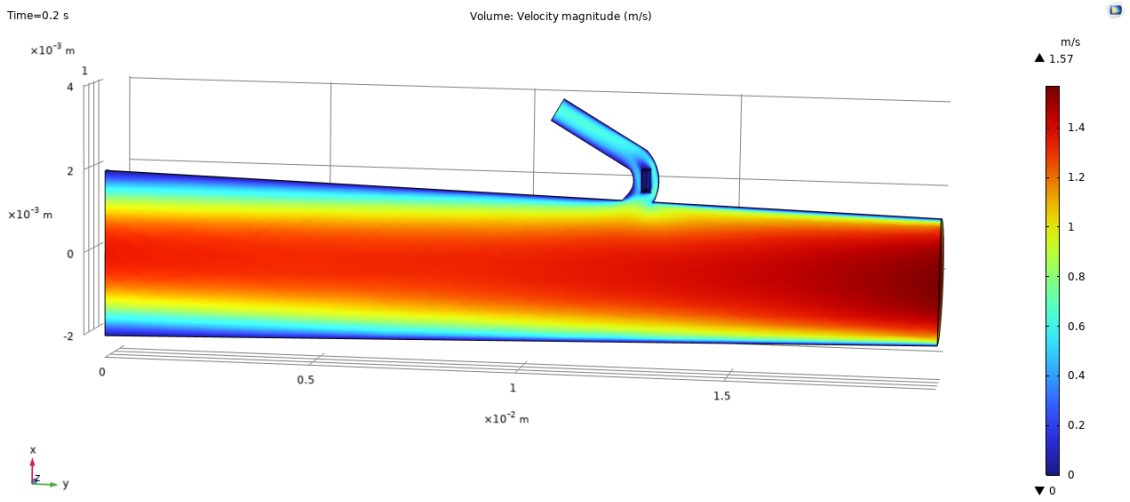

Figure 14: Simulation with the magnetic tip of 500 μm length

A notable observation regarding the magnetic tip is that the flow on the outer part of the curve is almost unaffected by its presence, while the flow is blocked on the inner part of the curve. Additionally, the flow quickly returns to its original speed after passing the magnetic tip.

According to Figure 15 the average flow rate is $4.41 \cdot 10^{-6}$ $[m^3/s]$. The average flow rate in the ophtalmic artery is 0.0525 $[m^3/s]$.

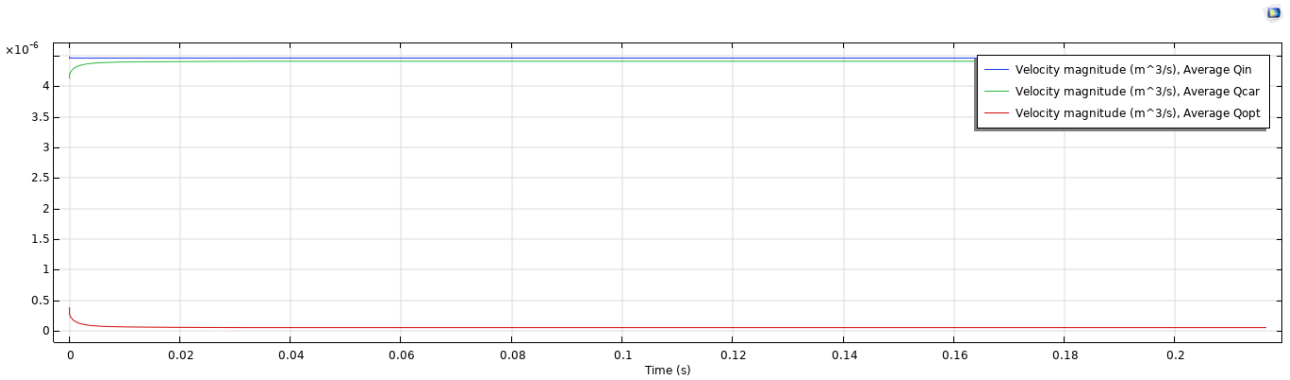

Figure 15: Average velocity at the inlet and outlets of the model

3.3.3 Simulation with clinical catheter of $0.4\ \mu m$

To gain a better understanding of how a catheter affects fluid dynamics when it obstructs blood flow, two simulations will be conducted.
In the first simulation, the catheter will extend through the entire length of the ophthalmic artery. This setup (Figure 16) will help us analyze the impact when the catheter spans the full vessel.
In the second simulation, the catheter will stop at the same point as the magnetic tip (Figure 17).

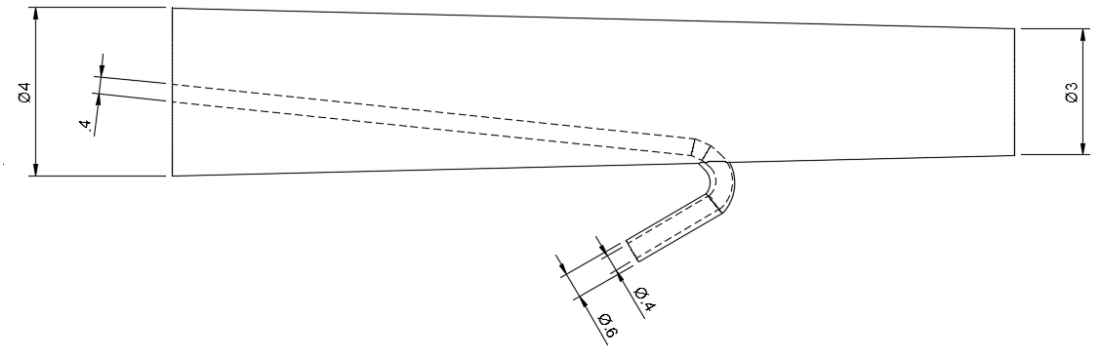

Figure 16: Model with full span clinical catheter CAD

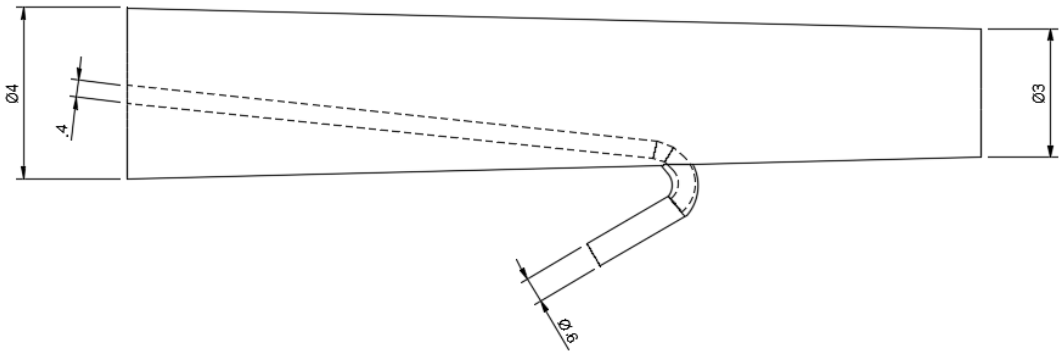

Figure 17: Model with mid span clinical catheter CAD

Full span catheter:
We can observe in Figure 18 that the flow is significantly slower in the ophthalmic artery due to the catheter blocking most of the section.
According to Figure 19, the average flow rate in the carotid section is $4.459 \cdot 10^{-6}$ $[m^3/s]$. The average flow rate in the opthalmic section is $0.0082 \cdot 10^{-6}$ $[m^3/s]$.

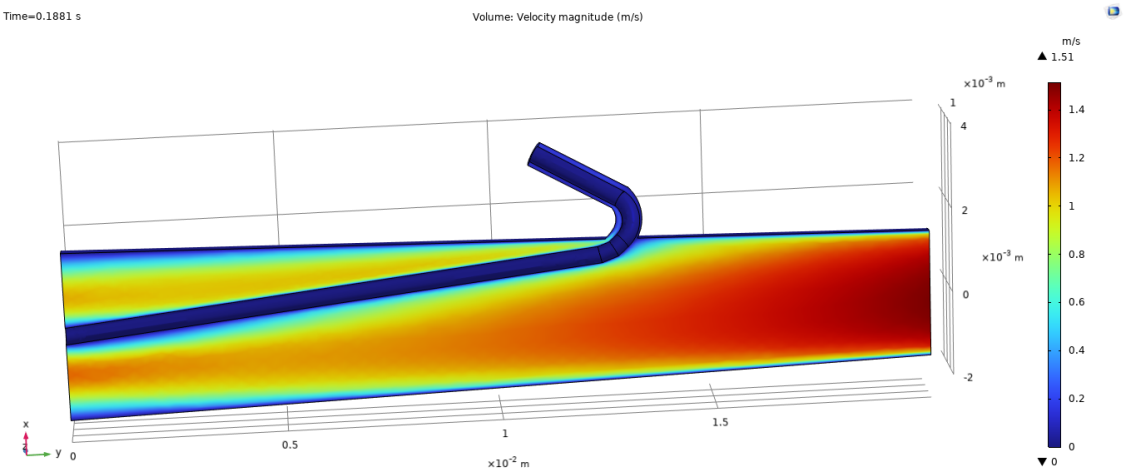

Figure 18: Simulation of the discretised model with the catheter

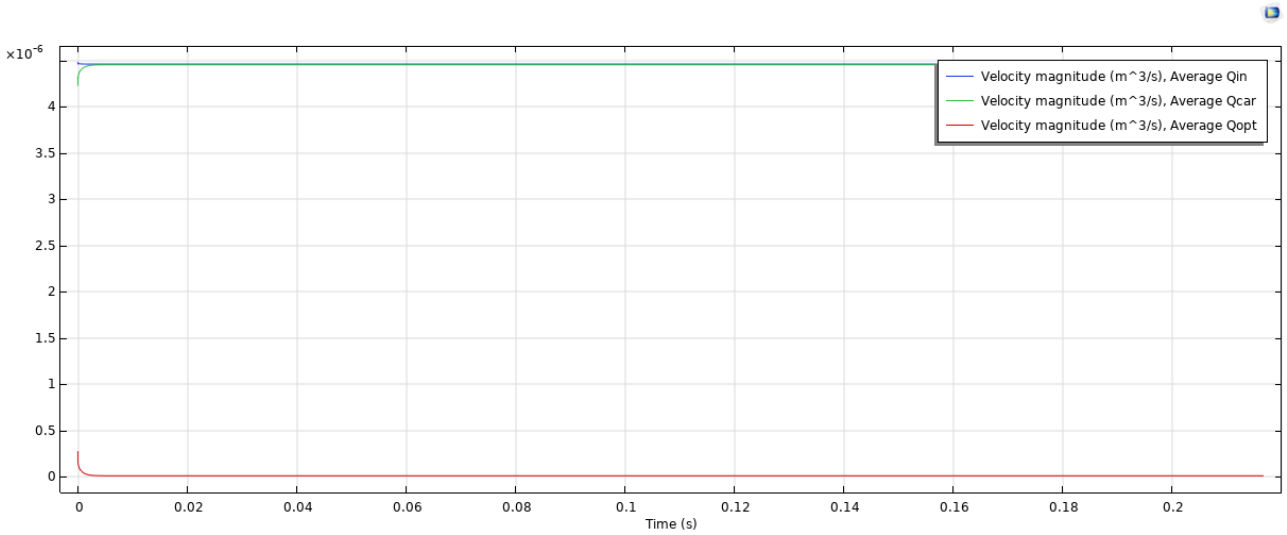

Figure 19: Average velocity at the inlet and outlets of the model

Mid span catheter:
We can observe in Figure 20 that the flow is significantly slower in the ophthalmic artery due to the catheter blocking most of the section.
According to Figure 21, the average flow rate in the carotid section is $4.445 \cdot 10^{-6}$ $[m^3/s]$. The average flow rate in the opthalmic section is $0.0182 \cdot 10^{-6}$ $[m^3/s]$.

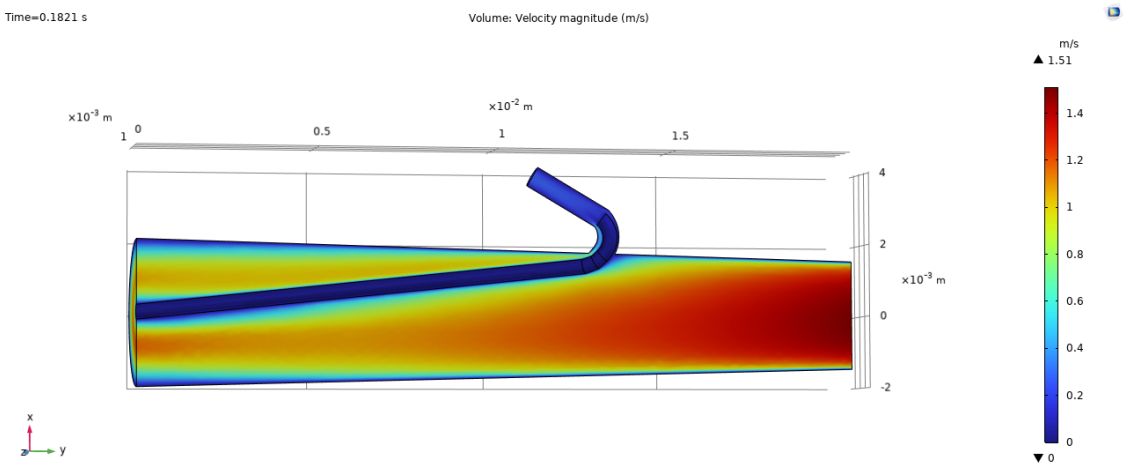

Figure 20: Simulation of the discretised model with the catheter

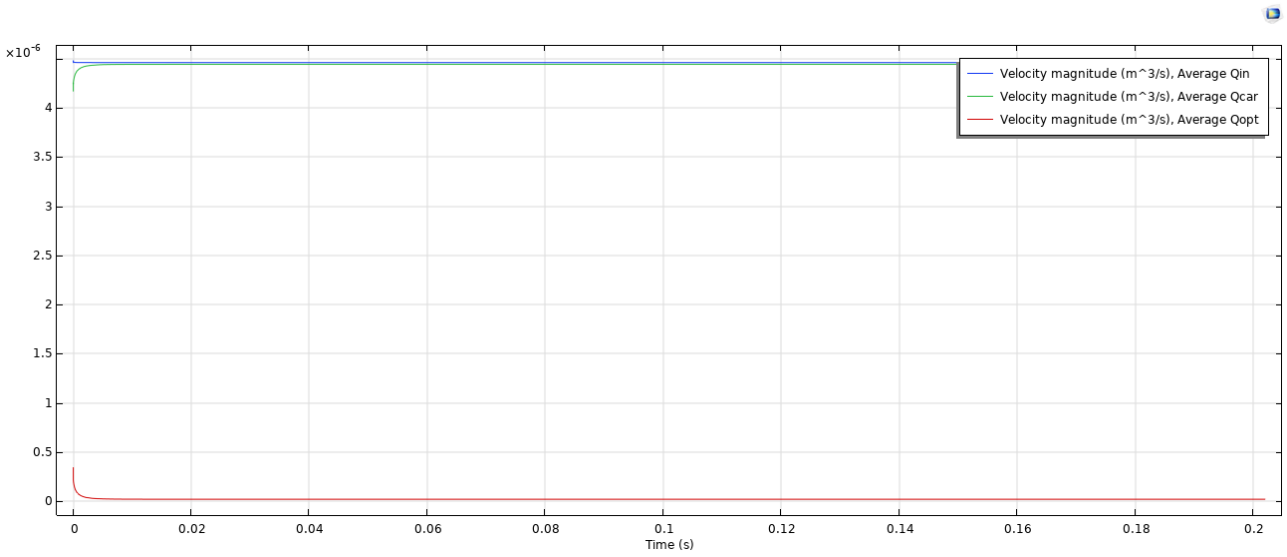

Figure 21: Average velocity at the inlet and outlets of the model

3.3.4 Comparison and results

Outlet flow rate	Carotid $\dot{Q}_{car}$ $[m^3/s]$	Ophtalmic $\dot{Q}_{opt}$ $[m^3/s]$
Control	$4.40 \cdot 10^{-6}$	$0.0616 \cdot 10^{-6}$
Magnetic tip	$4.41 \cdot 10^{-6}$	$0.0525 \cdot 10^{-6}$
Full span Catheter	$4.46 \cdot 10^{-6}$	$0.0082 \cdot 10^{-6}$
Mid span Catheter	$4.45 \cdot 10^{-6}$	$0.0182 \cdot 10^{-6}$
Literature	$4.45 \cdot 10^{-6}$	$0.114 \cdot 10^{-6}$

This table highlights the impact of different instruments on the flow rate in the ophthalmic artery. In the control simulation, the flow rate in the ophthalmic artery is $0.0616 \cdot 10^{-6}$ $[m^3/s]$. When using the full span catheter, this flow rate decreases significantly to $0.0082 \cdot 10^{-6}$ $[m^3/s]$, indicating that the full span catheter blocks 86.9% of the flow. Similarly, the mid span catheter blocks 70.4% of the flow, with a flow rate of $0.0182 \cdot 10^{-6}$ $[m^3/s]$. In contrast, the magnetic tip results in a flow rate of $0.0525 \cdot 10^{-6}$ $[m^3/s]$, blocking only 17.3% of the flow.

4 Test simulation with blood

To make the model more accurate, the material imput in Comsol need to follow as close as possible the blood physics in the vessel.
To achieve this, a material must be created manually in Comsol with blood properties by selecting ***Non-Newtonian Flow*** and then ***Carreau Model***.

4.1 Model properties

Assumptions

- Blood flow is a Poiseuille flow ([4])
  → incompressible, uniform, viscous liquid
- Blood viscosity follows the Carreau-Yasuda model ([2])

Properties

- Blood temperature : $T_b = 37° = 310K$
- Blood density : $\rho_b = 1060\ \text{kg.m}^{-3}$
- Apparent viscosity (Carreau model) : $\mu_{app} = \mu_\infty + (\mu_0 - \mu_\infty)[1 + (\lambda\hat{\gamma})^\alpha]^{\frac{n-1}{\alpha}}$
  where λ is a parameter with the unit of time, μ_0 is the zero shear rate viscosity, μ_∞ is the infinite shear-rate viscosity, and n is a dimensionless parameter.

The paremeters for the apparent viscosity are found in [1]. we chose the ones for 45% htc.

	Parameters			
Hct	η_0 (P)	λ (s)	n	η_∞ (P)
25%	0.178	12.448	0.330	0.0257
45%	1.610	39.418	0.479	0.0345
65%	8.592	103.088	0.389	0.0802

Figure 22: Carreau model parameters with different hematocrits

However, this model could not be implemented due to an error that occured after changing the fluid from water (Newtonian) to the Non-Newtonian fluid option : "**failed to find consistent initial values. last time step not converged.**". This issue did not arise when the simulation material was water, indicating that the change in material properties is likely the cause.
Several attempts were made to resolve this issue, unfortunately, these changes did not resolve the error :

- Changing Initial Values
- Following COMSOL Documentation on this specific error.

The trouble with using a non-Newtonian fluid really shows how tricky it can be to simulate these materials accurately. Unlike water, which behaves consistently, non-Newtonian fluids like blood change their properties depending on the flow conditions. This makes them much harder to model correctly.

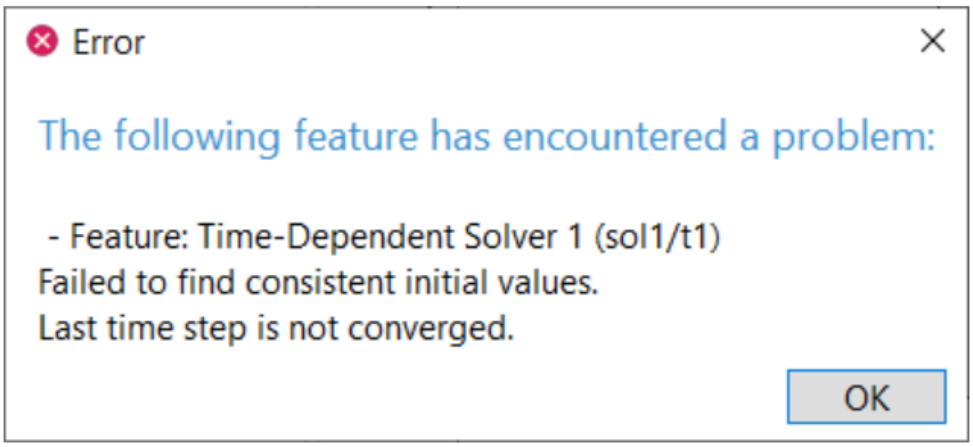

Figure 23: Error

5 Conclusion

As shown in the table in section 3.3.4, the flow blocked by the magnetic tip is significantly less than the flow blocked by the catheter. The magnetic tip blocks only 17.3% of the flow, while the catheter blocks between 70.4% and 86.9% of the flow.These findings are significant as they demonstrate that the magnetic tip has a considerably lesser impact on the flow within the ophthalmic artery compared to the catheter. The reduced obstruction caused by the magnetic tip suggests that it has potential to be developped into a device that could be used in operations involving the ophthalmic artery, as it maintains a higher flow rate, closer to the natural state. This is critical for ensuring adequate blood flow and minimizing the risk of complications during medical procedures.

Additionally, the flow rates in the carotid artery remain relatively unchanged across the different simulations, indicating that the procedure primarily affects the ophthalmic artery. Overall, the results validate the safety and efficacy of the magnetic tip, making it a promising tool for procedures involving the ophthalmic artery.

It is important to note that multiple factors could have introduces errors in the results.
Firstly, these results were obtained using water as the simulation medium. Due to time constraints, simulations could not be performed with blood, a non-Newtonian fluid, which would provide more accurate and realistic data. Future work should include simulations with blood properties to increase the accuracy of the model.
Secondly, the three-elements Windkessel model present discrepencies compared to litterature in regards of the ophtalmic arteries. This might be due to the accuracy of the simple model geometry, we should also consider the option that the model implementation in Comsol is not ideal and could be improved. While the order of magnitude is the same as in litterature, there could be room for improvement.

6 Future work

There are several tasks for future research and development to continue the current project.

1. **Simulation with Blood Properties and the Carreau-Yasuda Model:**

   Implementing the Carreau-Yasuda model to more accurately simulate the non-Newtonian properties of blood. This requires resolving the current errors preventing its implementation. The Carreau-Yasuda model will provide a more realistic representation of blood flow, accounting for its shear-thinning behavior.

2. **Simulation with the Segmented Vessel:**

   Using the segmented vessel geometry for simulations to obtain more accurate data. This would enhance the validity of the simulation results and their applicability to real-world scenarios.

3. **Simulation with Different Sizes of Magnetic Tip:**

   Conducting simulations with varying sizes of the magnetic tip to assess the impact of different lengths and radii on the flow dynamics. Understanding how different dimensions affect flow can help optimize the design of the magnetic tip for safer and more effective use in medical procedures.

4. **Data based on children patients:**

   The values from litterature used in this project are mostly coming from adults. However, retinoblastoma impacts mostly young children under the age of 5 ([6]). Thus it would be better for future works to use data from children anatomy.

5. **Improvement of the model**

   The current model used, the three-elements Windkessel model, present discrepencies with litterature in regards of the ophtalmic artery. Improving the implementation of the model or finding a better model altogether should also be taken in consideration for future works.

Addressing these areas will contribute to more robust and reliable simulation models. These steps are crucial for improving the accuracy of the simulations and their relevance to clinical applications.

7 Acknowledgements

Many thanks to Georgios Rovas for his insights on cardiovascular subjects and for providing values and models that greatly assisted this work.
Thank you to Artur Banach and Julian Raub for their constant support throughout this project.

References

[1] Khalid Ambarki, Per Hallberg, Gauti Jóhannesson, Christina Lindén, Laleh Zarrinkoob, Anders Wåhlin, Richard Birgander, Jan Malm, and Anders Eklund. Blood Flow of Ophthalmic Artery in Healthy Individuals Determined by Phase-Contrast Magnetic Resonance Imaging. *Investigative Ophthalmology Visual Science*, 54(4):2738–2745, 04 2013.

[2] Joshua Boyd, James M Buick, and Simon Green. Analysis of the casson and carreau-yasuda non-newtonian blood models in steady and oscillatory flows using the lattice boltzmann method. *Physics of Fluids*, 19(9), 2007.

[3] B C Chu, A Narita, K Aoki, T Yoshida, T Warabi, and K Miyasaka. Flow volume in the common carotid artery detected by color duplex sonography: an approach to the normal value and predictability of cerebral blood flow. *Radiat. Med.*, 18(4):239–244, July 2000.

[4] Gilbert T Feke, Hiroshi Tagawa, Dana M Deupree, Douglas G Goger, Jerry Sebag, and JJ Weiter. Blood flow in the normal human retina. *Investigative ophthalmology & visual science*, 30(1):58–65, 1989.

[5] Leif Rune Hellevik. Cardiovascular biomechanics, 6.2.2 three-element windkessel model, 2018.

[6] Dietmar R Lohmann and Brenda L Gallie. *Retinoblastoma*. University of Washington, Seattle, September 2023.

[7] Philippe Reymond, Fabrice Merenda, Fabienne Perren, Daniel Rüfenacht, and Nikos Stergiopulos. Validation of a one-dimensional model of the systemic arterial tree. *Am. J. Physiol. Heart Circ. Physiol.*, 297(1):H208–H222, July 2009.

[8] Prin Rojanapongpun and Stephen M Drance. Velocity of ophthalmic arterial flow recorded by doppler ultrasound in normal subjects. *Am. J. Ophthalmol.*, 115(2):174–180, February 1993.